Available online at www.sciencedirect.com
ScienceDirect
Ceramics International 38 (2012) 747–753
CERAMICS INTERNATIONAL
www.elsevier.com/locate/ceramint

Effect of NiO content on structural, surface and catalytic characteristics of nano-crystalline NiO/CeO_2 system

N.M. Deraz

Chemistry Department, College of Science, King Saud University, Riyadh, Saudi Arabia

Received 22 July 2011; received in revised form 27 July 2011; accepted 29 July 2011
Available online 5th August 2011

Abstract

The NiO/CeO_2 nano-composite catalysts containing different nickel content prepared by impregnation method have been characterized by XRD and TEM. The surface and catalytic properties of Ni/Ce mixed oxide solids were determined by nitrogen adsorption at −196 °C and catalytic conversion of isopropanol at different temperatures. These composites can be described as a mixture of nickel oxide and ceria modified by the insertion of a part of nickel in the ceria lattice. The size of the nickel oxide varies considerably from clusters to a crystallized material, depending on the amount of nickel oxide. From the characterization of the composites, it was concluded: at low Ni loading, the ceria surface is gradually covered with the dispersed NiO species. At higher loading, highly dispersed NiO, well crystalline nickel oxide and Ni–Ce–O solid solution coexist.

It was verified that the structural, morphological, surface and catalytic properties could be influenced by nickel loading. This treatment led to a slightly increase in the crystallite size of ceria particles. On the other hand, the augmentation in the nickel content brought about an increase in the crystallite size, lattice constant and unit cell volume of nickel oxide. The nickel loading brought about an increase in the formation of Ni–Ce–O solid solution with subsequent creation of oxygen vacancies.

Keywords: XRD; TEM; NiO/CeO_2 composite; Surface area; Catalytic activity; Loading

1. Introduction

Transition metal oxide based nano-composite catalysts are extensively studied with the objective of replacing much more expensive noble metals. The most of supported catalysts contain active phases in the form of nanometer-sized particles, of metal or oxide, dispersed over the surface of support material. The support material in supported catalysts brought about an increase in the stabilization of metal or oxide with subsequent modifications in the surface and catalytic properties of these catalysts [1]. The metal–support interactions that can be established between the supported phase and the support can further modulate the intrinsic surface properties of the supported phase [2]. It is generally acknowledged that reducible oxides are good candidates to exhibit this kind of phenomenon [2]. Cerium (IV) oxide has been extensively studied because of its interesting redox and high dispersive properties [3–6]. Oxygen atoms in CeO_2 units are very mobile and leave easily the ceria lattice, giving rise to a large variety of non-stoichiometric oxides with two limiting cases CeO_2 and Ce_2O_3. As a result, ceria has an insulator behavior in the stoichiometric oxidized state CeO_2 and becomes conductor in the reduced state CeO_{2-x}. The non-stoichiometric oxides can be produced by chemical reduction at temperatures much higher than ambient ($\geq$620 K) in hydrogen [6].

Cerium-based nano-composite catalysts containing transition metals have attracted increasing attention in recent years due to their high oxygen storage capability [7–17]. Various studies have shown that the redox properties can be considerably enhanced if additional elements are introduced into the CeO_2 lattice [14–22]. Because 4f orbital's give them a surplus of atomic electron valence, rare earth elements can be used to promote the activity and stability of metal catalysts [19]. NiO/CeO_2 catalysts have been studied in many hydrogenation reactions [19] by taking the advantage of their redox property. The beneficial association between species based on both nickel and cerium in oxidized and reduced states has been evidenced [12,13].

The major objective of the present study is to investigate the effect of NiO-loading on the structural, morphological and

E-mail address: nmderaz@yahoo.com.

0272-8842/$36.00
doi:10.1016/j.ceramint.2011.07.068

surface properties of NiO/CeO_2 nano-composite catalyst prepared by wet impregnation method. The nickel–ceria interaction was characterized by XRD and TEM techniques. Since the metal–support interaction often plays a key role in determining the details of surface properties; another objective of this investigation is to establish the relationship between the surface characteristics and the metal–support interaction by applying the NiO/CeO_2 nano-composite catalysts calcined at various temperatures to N_2 adsorption.

2. Experimental

2.1. Composite catalysts preparation

Five NiO/CeO_2 catalyst samples were prepared by impregnating a known weight of finely powdered ceria solid with calculated amounts of nickel nitrate dissolved in the least amount of distilled water enough to make a paste. The paste was dried at 100 °C in air until it was constant in weight and was then subjected to heat treatment for 4 h at 450 °C in air. The nickel concentrations were 4, 8, 15, 21 and 26 wt% NiO during the catalyst preparation. The chemicals employed were of analytical grade and supplied by BDH Company.

2.2. Composite catalysts characterization

An X-ray measurement of various mixed solids was carried out using a BRUKER D8 advance diffractometer. The patterns were run with Cu K_α radiation at 40 kV and 40 mA with scanning speed in 2θ of 2° min^{-1}.

The crystallite size of CeO_2 and NiO phases present in the investigated solids was calculated via X-ray diffraction line broadening of main planes (1 1 1) and (2 0 0) related to cerium and nickel oxides, respectively, using Scherrer equation [23].

$$D = \frac{B\lambda}{\beta \cos\theta} \quad (1)$$

where D is the mean crystallite size of the phases under investigation, B is the Scherrer constant (0.89), λ is the wave length of X-ray beam used, β is the full-with half maximum (FWHM) of diffraction and θ is the Bragg's angle. The lattice constant (a) was calculated using inter-planar spacing (d) values and Miller indices ($h\,k\,l$) values i.e. $a = d(h^2 + k^2 + l^2)^{1/2}$. The unit cell volume ($V$) was equal to the cube of lattice constant i.e. $V = a^3$.

Transmission electron micrographs (TEM) were recorded on JEOL TEM-1230 electron microanalysis, respectively. The samples were dispersed in ethanol and then treated ultrasonically in order disperse individual particles over a gold grids.

2.3. Surface properties

The surface characteristics of various nanocomposite catalysts, namely, The specific surface area (S_{BET}), total pore volume (V_p) and mean pore radius ($\bar{r}$) were determined from nitrogen adsorption isotherms measured at −196 °C, using Nova 2000, Quanta Chrome (commercial BET unit). Before undertaking such measurements, each sample was degassed under a reduced pressure of 10^{-5} Torr for 2 h at 200 °C.

2.4. Catalytic behavior

The catalytic conversion of isopropanol was carried out over various catalysts at temperatures within 250 and 450 °C using a flow method. The reactant (spec. pure isopropanol) was introduced using a micro-dose pump (Unipan 335A) via pure nitrogen gas flowing at a rate varying between 7.2 and 18.7×10^{-2} ml min^{-1}. The catalyst sample (100 mg) was introduced into a quartz reactor and put between two silica wool beds. The catalyst sample was activated by heating at 400 °C for 2 h in a current of dry air free from CO_2 then cooled down to the temperature of the catalytic reaction. The gaseous and liquid products of the catalytic reaction were analyzed using programmed gas–liquid chromatograph (Perkin-Elmer 8600) double flame ionization detector on a column 5% CW 1540 on CSORB (Gaw-DMCs) which was applied for alcohols using pure nitrogen as a carrier gas.

3. Results and discussion

3.1. XRD analysis

The XRD patterns of ceria based nano-composites containing 4, 8, 15, 21 and 26 wt% NiO, calcined at 450 °C for 4 h, were determined and shown in Fig. 1. For each sample, the diffraction patterns evidenced the nano-crystalline CeO_2 phase was observed. The ceria is cubic system with space group $Fm3m$. As seem from Fig. 1, the diffraction of the 4 wt% NiO/CeO_2 sample includes all the diffraction peaks of CeO_2 with the absence of NiO peaks depending on the amount of NiO which is very small beyond the detection limit of X-ray diffraction. This observation suggests fine dispersion of NiO on the surface of ceria and/or solid solution formation [24–26]. However, the diffractograms of the catalysts containing 8–26 wt% NiO consisted of the diffraction peaks of CeO_2 as the major phase, having different degrees of crystallinity depending on the NiO content, besides some diffraction peaks of NiO phase. The heights of NiO peaks increased when the nickel oxide concentration was increased from 8 to 26 wt% NiO.

Loading of NiO on the ceria surface could be lead to some modifications of their structural characteristics i.e. the degree of crystallinity, crystallite size (D), the lattice constant (a), unit cell volume (V) of the Ni and Ce oxides. Analysis of the X-ray data allowed these characteristics to be determined for the investigated catalysts. The computed values of these parameters are listed in Table 1. Examination of the data listed in Table 1 indicates the following: (i) the addition of NiO on the surface of ceria increased the degree of the crystallinity of CeO_2 as demonstrated by the increase in the peak height of the main diffraction line of the ceria phase. This increase was inversely proportional to the amount of nickel oxide added from 8 to 26 wt% NiO. The maximum increase in the degree of crystallinity of CeO_2 due to the loading with 8 wt% NiO attained the value of 43%. (ii) Treatment of ceria

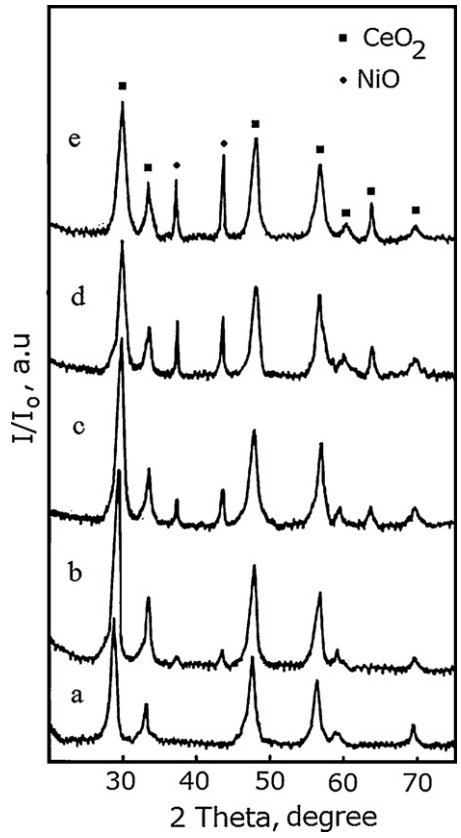

Fig. 1. X-ray diffractograms of NiO/CeO_2 nano-composites calcined at 450 °C. NiO concentrations: (a) 4; (b) 8; (c) 15; (d) 21 and (e) 26 wt%.

with different NiO content followed by calcination at 450 °C led to a significant increase in the crystallite size of NiO phase. However, this treatment brought about a slightly increase in the crystallite size of ceria. This increase may be considered as a measure of the enhanced decrease in the degree of dispersion of NiO phase due to the loading process. The maximum decrease in the dispersion degree of NiO, due to loading with NiO, attained 96% in the case of the sample containing 26 wt% NiO. (iii) Increasing the NiO content brought about an increase in the lattice constant '*a*' of the ceria crystallites. This behavior may be attributed to the dissolution of a proportion of the nickel oxide in the CeO_2 lattice with subsequent formation of solid solution. Indeed, nickel loading led to a shift in the position of the diffraction peaks of both CeO_2 and NiO towards the higher Bragg's angle indicating the presence of such the solid solution on the catalysts surface [24–26].

Adopting Kröger notations [27] dissolution of NiO in the ceria lattice take place according to the following reactions:

$$NiO + 2Ce^{4+} \rightarrow Ni(Ce^{3+}) + 2Ce^{3+} + 1/2O_2 \quad (2)$$

$$NiO + 2Ce^{4+} \rightarrow 2Ni_{\Delta} + 2Ce^{3+} + 1/2O_2 \quad (3)$$

$$NiO + Ce^{4+} \rightarrow 2Ni(Ce^{4+}) + Ce^{4+} + A.V. \quad (4)$$

where Ni_{Δ} are divalent nickel ions retained in the interstitial positions; $Ni(Ce^{4+})$ and $Ni(Ce^{3+})$ are divalent nickel ions located in the positions located in the positions of host tetravalent cerium ions in the CeO_2 lattice and A.V. is anionic vacancy.

Dissolution of NiO via reactions (2) and (3) is accompanied by the transformation of some of the Ce^{4+} ions to Ce^{3+} ions (the ionic radius of these ions being 0.087 and 0.102 nm, respectively) [28]. This process is normally accompanied by an increase in the lattice constant of CeO_2. The possible creation of anionic vacancies in CeO_2 due to loading followed by calcination at 450 °C might result in the contraction in its crystal lattice which did not observed experimentally. This indicates the increase in the metal–support interaction between nickel and cerium oxides forming solid solution.

The observed increase in the value of the lattice constant of NiO upon loading it on the ceria surface may be attributed to the agglomeration of NiO particles and also to transformation of some of the Ni^{3+} ions to Ni^{2+} ions (the ionic radius of these ions being 0.062 and 0.78 nm, respectively) [28]. This reaction can be expressed as:

$$2Ni^{3+} + 2e^{-} + O^{2-} \rightarrow 2Ni^{2+} + 1/2O_2 \quad (5)$$

where Ni^{3+} ions exist in non-stoichiometric This solid-state reaction is normally accompanied by removal of a portion of excess oxygen present in non-stoichiometric NiO solid. In other words, the effective increase in crystallite sizes of both NiO and CeO_2 due to our experimental treatments involved in the present work could be attributed to conversion of some NiO to Ni_2O_3 and also some CeO_2 to Ce_2O_3 phases via CeO_2–NiO structure interaction. This indicates to presence of a synergistic mechanism between the nickel and cerium oxides [26]. The proposed mechanism in this case is as follows:

$$Ni_2O_3 \rightarrow 2NiO + 1/2O_2 \quad (6)$$

$$2NiO + 2CeO_2 \rightarrow Ni_2O_3 + Ce_2O_3 \quad (7)$$

$$Ce_2O_3 + 1/2O_2 \rightarrow 2CeO_2 \quad (8)$$

Table 1
The effects of nickel content on some structural parameters of nickel and cerium oxides involved in NiO/CeO_2 catalysts.

Concentration of NiO (wt%)	Calcin. temp. (°C)	CeO_2			NiO		
		D (nm)	*a* (nm)	*V* (nm^3)	*D* (nm)	*a* (nm)	*V* (nm^3)
4	450	15	0.5410	0.1583	–	–	–
8	450	16	0.5426	0.1597	25	0.4175	0.0728
15	450	16	0.5383	0.1559	39	0.4178	0.0729
21	450	16	0.5420	0.1592	42	0.4175	0.0728
26	450	17	0.5416	0.1588	49	0.4180	0.0730

The synergistic effect may be lead to modifications in the textural and morphological properties.

From the above observations we can conclude that some Ni^{2+} species diffuse into the fluorite structure forming a solid solution with ceria and also highly dispersed NiO on CeO_2 surface in case of the samples containing low nickel content. At high nickel content, solid solution, crystallized nickel oxide and highly dispersed NiO phases on ceria co-exist. Aggregated NiO on the surface of CeO_2 dominates at high Ni content (26 wt% NiO). Thus, the distribution of different Ni species strongly depends on the conditions of composite preparation.

It has been discovered that many salts and oxides can disperse spontaneously onto the surfaces of supports to form a monolayer. Studies of more different systems and the characteristics obtained by XRD, XPS, Raman, EXAFS, TPD and TPR demonstrate that this is quite a widespread phenomenon [24]. For a salt or an oxide dispersed on a support, there is a monolayer dispersion threshold [24,25]. When the loading is lower than the threshold, the salt or oxide will be in a monolayer state and XRD-undetectable. Once the loading exceeds the threshold, in most situations, the surplus salt or oxide will remain as a separate crystalline phase in the system together with its monolayer phase and give XRD peaks. XRD quantitative phase analysis is employed by many authors to measure the residual crystalline salt or oxide versus loading and to determine the dispersion threshold of the salt or oxide on the support by an extrapolation method [24,25]. We think that, with respect to the case of NiO/CeO_2, NiO has dispersed onto the surface of CeO_2 as a monolayer. The XRD peak intensity ratio of NiO (2 0 0) reflection to CeO_2 (1 1 1) reflection can be taken as the relative amount of residual crystalline NiO in the samples of NiO/CeO_2. The ratio of $I_{(2\,0\,0)}/I_{(1\,1\,1)}$ as a function of NiO content is shown in Fig. 2. It can be seen from this figure that the nickel oxide will be in a monolayer state and XRD-undetectable when the loading is lower than the dispersion threshold of 6 wt% NiO/CeO_2 nano-composite catalysts. The surplus NiO will remain as a separate crystalline phase in the system together with its monolayer phase and give XRD peaks when the loading exceeds the dispersion threshold.

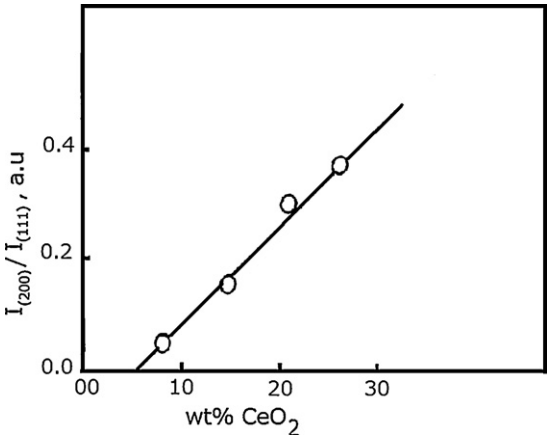

Fig. 2. XRD intensity ratio of $I_{NiO(200)}/I_{CeO_2(111)}$ versus NiO loading of NiO/CeO_2 nano-composites calcined at 450 °C.

3.2. Morphology characterization

TEM images of 4 wt%NiO/CeO_2 and 15 wt%NiO/CeO_2 nano-composites calcined at 450 °C are shown in Fig. 3a and b. All composites exhibit aggregated nano-particles with small and uniform sizes. From the results of Fig. 3a, it can be seen that the Ni particles (illustrated by black arrows) distributed within the nano-crystalline ceria matrix (illustrated by white arrows) which has an average particle size of 16 ± 1 nm. Increasing amounts of nickel oxide brought about an increase in the particle size of both nickel and cerium oxide as shown in Fig. 3b. These results are quite reasonable: crystallites grow with raising the degree of loading. We noticed that the shape of CeO_2 observed in TEM depends on the nickel content. The shape of particles seems to be more spherical. However, this treatment resulted in an increase in the incorporated amount nickel oxide in the ceria matrix with subsequent formation of the agglomerated nickel particles for the sample containing high Ni content.

To complete the information, electronic micro-diffraction was used to determine the chemical structure of the small

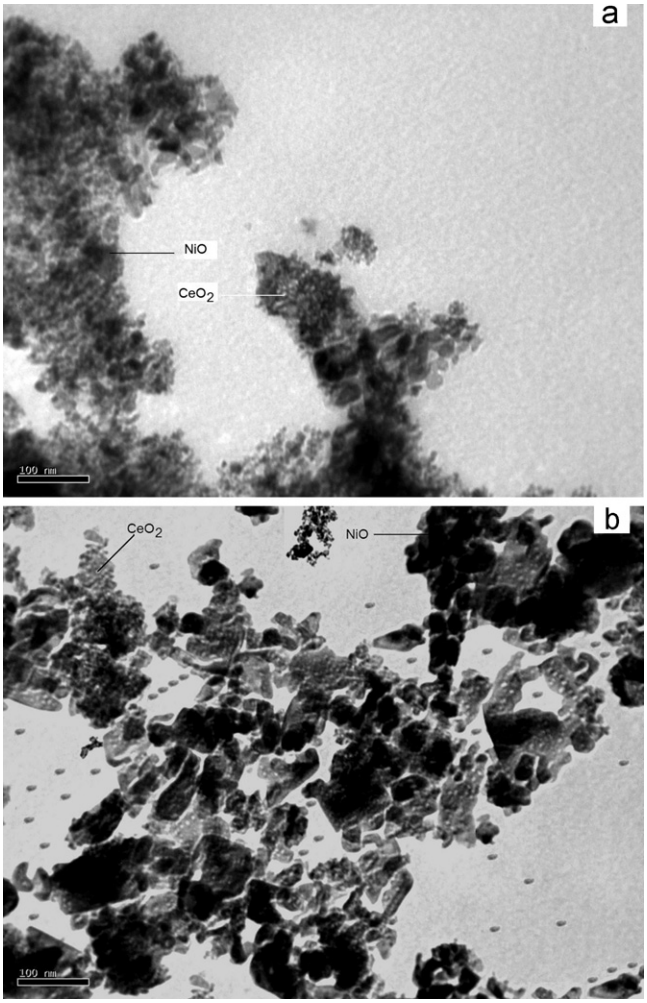

Fig. 3. TEM images of various NiO/CeO_2 nano-composites calcined at 450 °C. NiO concentrations: (a) 4 and (b) 15 wt%.

grains. The corresponding selected area electron diffraction (SAED) patterns of the mentioned samples are shown in Fig. 4a and b. All the diffraction spots corresponding to aggregates are generally distributed on circles. Whatever the sample, the circles related to the micro-diffraction of CeO_2 are continuous in agreement with the homogeneity of the CeO_2 grains observed in TEM images. The punctuated diagrams are related to NiO for the NiO/CeO_2 sample containing 4 or 15 wt% NiO suggesting that the corresponding particles are oriented and/or inhomogeneous in size (Fig. 4a and b). In 4 wt% NiO/CeO_2 sample calcined at 450 °C, the circles corresponding to the micro-diffraction of NiO are not complete and only few spots are visible in agreement with the low quantity of nickel in this sample (Fig. 4a). Increasing the amount of NiO added led to an increase in the spots on the diffraction circles for the 15 wt% NiO/CeO_2 specimen indicating presence of the agglomerated nickel species on ceria surface (Fig. 4b). According to the diffraction patterns in Fig. 5a and b, the measured lattice constants and inter-planar spacing (d_{hkl}) of CeO_2 and NiO agree with those in the XRD results.

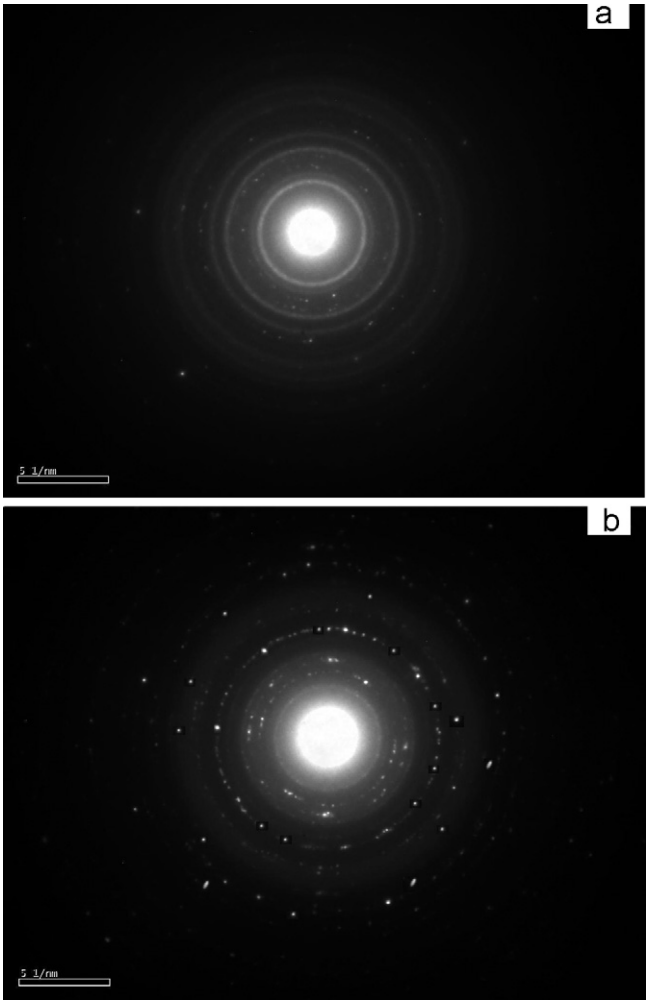

Fig. 4. The corresponding selected area electron diffraction images of various NiO/CeO_2 nano-composites calcined at 450 °C. NiO concentrations: (a) 4 and (b) 15 wt%.

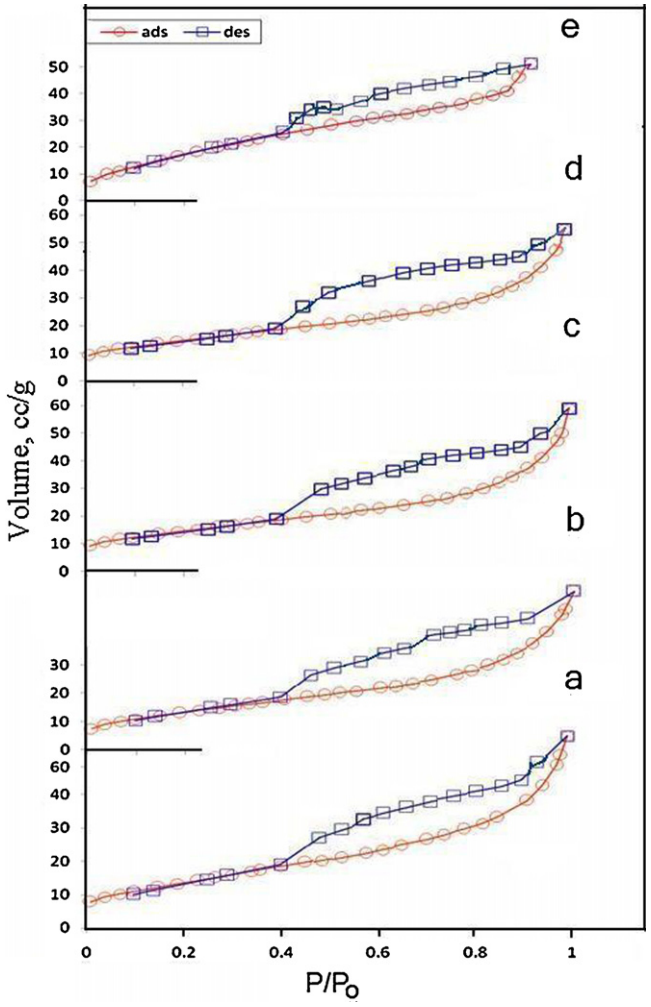

Fig. 5. N_2 adsorption/desorption isotherms for NiO/CeO_2 system calcined at 450 °C. NiO concentrations: (a) 4; (b) 8; (c) 15; (d) 21 and (e) 26 wt%.

3.3. Surface properties

The different surface characteristics, namely, specific surface area (S_{BET}), total pore volume (V_p) and mean pore radius ($\bar{r}$), of the various composites were determined from nitrogen adsorption isotherms conducted at −196 °C. Representative adsorption/desorption isotherms for nitrogen on various sample investigated are depicted in Fig. 5. All the isotherms displayed common characteristics, being similar in the shape to type II of Brunauer's classification [29].

The results obtained are given in Table 2. Inspection of Table 2 reveals that NiO-loading resulted in a measurable increase in the S_{BET} (44%), V_p (7.8%) with subsequent a decrease in the $\bar{r}$ (26.5%) for the composite containing 26 wt% NiO followed by heating at 450 °C. The induced increase in the S_{BET} and V_p of the NiO/CeO_2 system due to the loading with NiO followed by heating at 450 °C can be attributed to the creation of pores produced from liberation of excess nitrogen oxides gas during the thermal decomposition of nickel nitrate [25,26].

More detailed information on the porosity is available from the representative pore volume distribution curves shown in Fig. 6 constructed by plotting D_{Vp}/D_r against the pore radius [30]. It is

Table 2
The surface properties of NiO/CeO_2 catalysts containing different amounts of nickel oxide.

Concentration of NiO (wt%)	Calcin. temp. (°C)	S_{BET} (m^2/g)	V_p (cm^3/g)	$\bar{r}$ (nm)
4	450	50	0.85101	3.40
8	450	51	0.08648	3.40
15	450	53	0.09110	3.50
21	450	60	0.09201	3.10
26	450	72	0.09160	2.50

seen that the investigated solids exhibited one model distribution in which most of the pores were located in the meso-pore range. However, the maxima of the pore volume distribution curves are located at range of 1.3–1.8 nm. The heights of these distribution curves increase by increasing the amounts of nickel oxide added indicating an increase in the porosity of the investigated solids. This increase parallels the increase in surface area.

3.4. Catalytic performance

The catalytic conversion of isopropanol over the as prepared catalysts was carried out at temperatures 250–450 °C using a flow system. These catalysts included various amounts of nickel oxide acted as dehydrogenation and dehydration catalysts producing acetone and propene. The effects of the extent of loading on the catalytic activity and selectivity are better represented by plotting the values of activity (expressed as the total conversion) and selectivity for the different catalysts as a function of the amount of nickel oxide present in the system as shown Fig. 7.

Fig. 7a depicts the change of % total conversion of isopropanol carried out at 300 °C over the 4–26 wt% NiO/CeO_2 catalysts calcined at 450 °C. It can be seen from this figure that nickel loading of the investigated system led to a progressive increase in its activity as a function of the amount of nickel added.

Fig. 7b and c shows the influence of NiO loading of NiO/CeO_2 system on the selectivity towards the acetone and propene formation for the investigated reaction carried out at 300 °C over the investigated solids calcined at 450 °C. It is clear from this figure that the selectivity towards dehydration reaction of isopropanol conversion over NiO/CeO_2 system increased progressively by increasing the amount of nickel oxide up to 15 wt% NiO, and then decreased by increasing the content of NiO above this limit. Opposite effect was observed in the selectivity towards dehydrogenation.

The induced increase in the catalytic performance of the investigated catalysts by increasing the amount of nickel present in the samples from 4 to 26 wt% is to be expected as a result of the progressive increase in their specific surface areas and formation of Ni–Ce–O solid solution. In other words, the observed increase in the catalytic activity of Ni/Ce oxides system by increasing the extent of NiO loading could be attributed to an effective increase in the concentration of active sites involved in alcohol conversion.

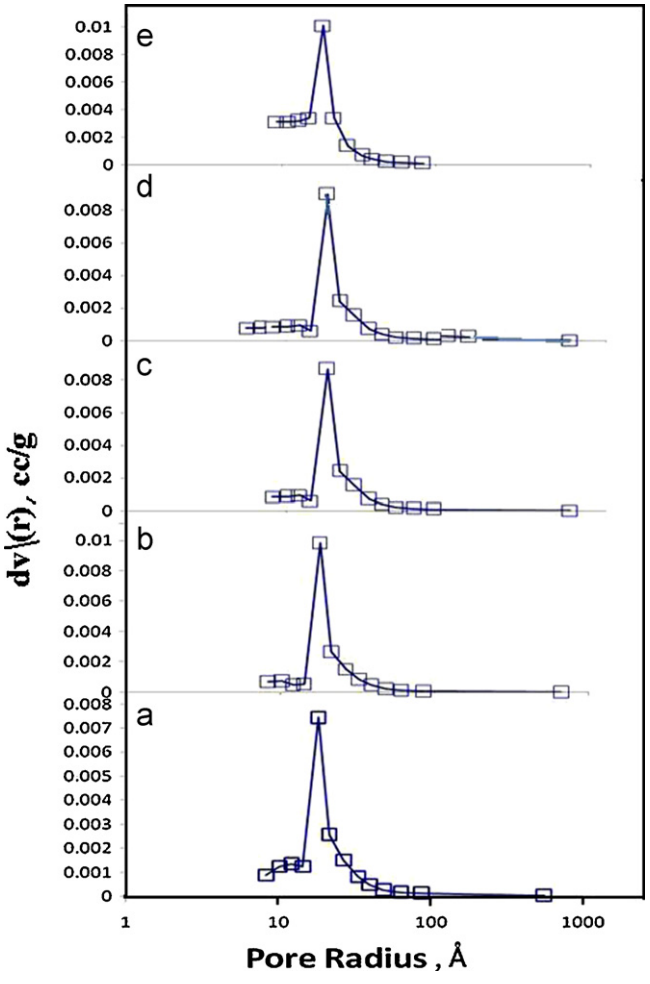

Fig. 6. Variation of dV/dr versus the pore radius for NiO/CeO_2 system calcined at 450 °C. NiO concentrations: (a) 4; (b) 8; (c) 15; (d) 21 and (e) 26 wt%.

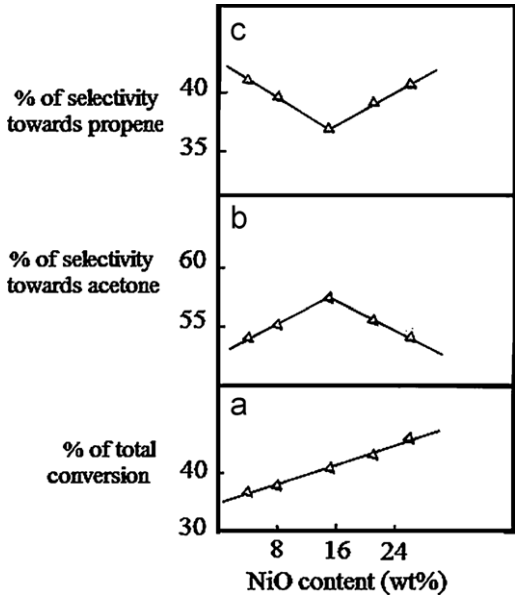

Fig. 7. Effect of the extent of NiO on: (a) percentage of total conversion, (b) selectivity towards acetone formation, (c) selectivity towards propene formation over different NiO/CeO_2 catalysts calcined at 450 °C.

Indeed, NiO/CeO_2 system acted as catalyst containing multi components, where the ceria itself has a measurable catalytic activity in alcohol conversion [31]. Ceria material behaves normally as dehydrogenation catalyst in isopropanol conversion reaction [31].

So, the decrease in the dehydrogenation selectivity due to our experimental treatment involved in the present work could be attributed to blocking a portion of active sites taking part in the dehydrogenation process by NiO. On the other hand, the increase in the dehydration selectivity may be due to a measurable increase in the concentration of surface Ni-species.

4. Conclusions

Nano-sized NiO/CeO_2 composites were prepared by wet impregnation method followed by calcination at 450 °C. The as prepared samples possessed large specific surface areas, small crystal sizes and high homogeneity of constituents even after calcination at 450 °C. Structure analysis revealed that NiO incorporated into the CeO_2 lattice, which remarkably modified the structural, morphological and textural properties of the final product. XRD technique suggests the presence of three different NiO species: highly dispersed NiO, nanocrystalline NiO and Ni–Ce–O solid solution i.e. dissolved Ni species in the CeO_2 lattice. All the as-prepared NiO/CeO_2 catalysts calcined at 450 °C with ultra fine particles exhibited highly surface area catalytic activity. The selectivity towards dehydrogenation is much bigger than those of dehydration reaction.

Acknowledgment

This project was supported by King Saud University, Deanship of Scientific Research, College of Science Research Centre.

References

[1] K. Hayek, H. Fuchs, B. Koltzer, W. Reicheil, G. Rupprechter, Studies of metal–support interactions with real and inverted model systems: reactions of CO and small hydrocarbons with hydrogen on noble metals in contact with oxides, Top. Catal. 13 (2000) 55.

[2] X. Tang, B. Zhang, Y. Li, Y. Xu, Q. Xin, W. Shen, CuO/CeO_2 catalysts: redox features and catalytic behaviors, Appl. Catal. A 288 (2005) 116.

[3] A. Laachir, V. Perrichon, A. Badri, J. Lamotte, E. Catherine, J.C. Lavalley, J. El Fallah, L. Hilaire, F. Le Normand, E. Quemere, G.N. Sauvion, O. Touret, Reduction of CeO_2 by hydrogen. Magnetic susceptibility and Fourier-transform infrared, ultraviolet and X-ray photoelectron spectroscopy measurements, J. Chem. Soc. Faraday Trans. 87 (1991) 1601.

[4] G. Jacobs, U.M. Graham, E. Chenu, P.M. Patterson, A. Dozier, B.H. Davis, Low-temperature water–gas shift: impact of Pt promoter loading on the partial reduction of ceria and consequences for catalyst design, J. Catal. 229 (2005) 99–512.

[5] C. Li, K. Domen, K.-I. Maruya, T. Onishi, Spectroscopic identification of adsorbed species derived from adsorption and decomposition of formic acid, methanol, and formaldehyde on cerium oxide, J. Catal. 125 (1990) 445.

[6] L. Filotti, A. Bensalem, F. Bozon Verduraz, G.A. Shafeev, V.V. Voronov, A comparative study of partial reduction of ceria via laser ablation in air and soft chemical route, Appl. Surf. Sci. 109–110 (1997) 249.

[7] A. Trovarelli, Catalytic properties of ceria and CeO_2-containing materials, Catal. Rev. Sci. Eng. 38 (1996) 439.

[8] P.L.J. Gunter, J.W. Niemantsverdriet, F.H. Riebeiro, G.A. Somorjai, Surface science approach to modeling supported catalysts, Catal. Rev. Sci. Eng. 39 (1997) 77.

[9] R.K. Usmen, G.W. Graham, W.L.H. Watkins, R.M. Mc Cabe, Incorporation of La^{3+} into a $Pt/CeO_2/Al_2O_3$ catalyst, Catal. Lett. 30 (1995) 53.

[10] B. Ernst, L. Hilaire, A. Kiennemann, Effects of highly dispersed ceria addition on reducibility, activity and hydrocarbon chain growth of a Co/SiO_2 Fischer–Tropsch catalyst, Catal. Today 50 (1999) 413.

[11] A. Bensalem, F. Bozon-Verduraz, M. Delamar, G. Bugli, Preparation and characterization of highly dispersed silica-supported ceria,, Appl. Catal. A 121 (1995) 81.

[12] G. Avgouropoulos, T. Ioannides, H.K. Matralis, J. Batista, S. Hocevar, $CuO–CeO_2$ mixed oxide catalysts for the selective oxidation of carbon monoxide in excess hydrogen, Catal. Lett. 73 (2001) 33.

[13] M. Daturi, E. Finocchio, C. Binet, J.C. Lavalley, F. Fally, V. Perrichon, H. Vidal, N. Hickey, J. Kaspar, Reduction of high surface area $CeO_2–ZrO_2$ mixed oxides, J. Phys. Chem. B 104 (2000) 9186.

[14] J. Kaspar, P. Fornasiero, M. Grazini, Use of CeO_2-based oxides in the three-way catalysis, Catal. Today 50 (1999) 285.

[15] T. Shido, Y. Iwasawa, Regulation of reaction intermediate by reactant in the water–gas shift reaction on CeO_2, in relation to reactant-promoted mechanism, J. Catal. 136 (1992) 493.

[16] G. Jacobs, E. Chenu, P.M. Patterson, L. William, D.E. Sparks, G. Thomas, Water–gas shift: comparative screening of metal promoters for metal/ceria systems and role of the metal, Appl. Catal. A 258 (2004) 203.

[17] I.A. Fisher, A.T. Bell, In situ infrared study of methanol synthesis from H_2/CO over $Cu/SiO_2$and $Cu/ZrO_2/SiO_2$, J. Catal. 178 (1998) 153–173.

[18] W. Shan, M. Luo, P. Ying, W. Shen, C. Li, Reduction property and catalytic activity of $Ce_{1-x}Ni_xO_2$ mixed oxide catalysts for CH_4 oxidation, Appl. Catal. A 246 (2003) 1.

[19] G. Wrobel, M.P. Sohier, A. D'Huysser, J.P. Bonnelle, J.P. Marcq, Hydrogenation catalysts based on nickel and rare earth oxides: Part II. XRD, electron microscopy and XPS studies of the cerium–nickel–oxygen–hydrogen system, Appl. Catal. A 101 (1993) 73.

[20] A.-G. Boudjahem, S. Monteverdi, M. Mercy, M.M. Bettahar, Study of nickel catalysts supported on silica of low surface area and prepared by reduction of nickel acetate in aqueous hydrazine, J. Catal. 221 (2004) 325.

[21] A.-G. Boudjahem, S. Monteverdi, M. Mercy, M.M. Bettahar, Study of support effects on the reduction of Ni^{2+} ions in aqueous hydrazine, Langmuir 20 (2004) 208.

[22] A.-G. Boudjahem, S. Monteverdi, M. Mercy, M.M. Bettahar, Nanonickel particles supported on silica. Morphology effects on their surface and hydrogenating properties, Catal. Lett. 97 (3–4) (2004) 177.

[23] B.D. Cullity, Elements of X-ray Diffraction, Addison-Wesly Publishing Co. Inc., 1976 (Chapter 14).

[24] D. Jiang, G. Pan, B. Zhao, G. Ran, Y. Xie, E. Min, Preparation of ZrO_2-supported MgO with high surface area and its use in mercaptan oxidation of jet fuel, Appl. Catal. A 201 (2000) 169.

[25] N.M. Deraz, Characterization and catalytic performance of pure and Li_2O-doped CuO/CeO_2 catalysts, Appl. Surf. Sci. 255 (2009) 3884.

[26] N.M. Deraz, Physicochemical, surface and catalytic properties of pure and ceria doped manganese/alumina system, Chin. J. Catal. 29 (8) (2008) 687.

[27] F.A. Kröger, Chemistry of Imperfect Crystals, North-Holand, Amsterdam, 1964.

[28] N.N. Greenwood, Inorganic Crystal Lattice Defects and Non-stoichiometry, Butterworths, London, 1964, p. 37.

[29] S. Brunauer, The Adsorption Of Gases and Vapors, Oxford University Press, Pinceton, NJ, USA, 1945, p. 150.

[30] S. Brunauer, R.Sh. MiKhail, E.E. Dodor, Pore structure analysis without a pore shape model, J. Colloid Interface Sci. 24 (1967) 451.

[31] N.M. Deraz, A. Alarifi, Structural, surface and catalytic properties of nanosized ceria catalysts, Adsorp. Sci. Technol. 27 (2009) 413.